Available online at www.sciencedirect.com
ScienceDirect
Journal of Solid State Chemistry 180 (2007) 98–105
JOURNAL OF SOLID STATE CHEMISTRY
www.elsevier.com/locate/jssc

Large-scale synthesis of single-crystal hexagonal tungsten trioxide nanowires and electrochemical lithium intercalation into the nanocrystals

Zhanjun Gu[a,b], Huiqiao Li[c], Tianyou Zhai[a], Wensheng Yang[d], Yongyao Xia[c], Ying Ma[a,*], Jiannian Yao[a,*]

[a]*Key Laboratory of Photochemistry, Beijing National Laboratory for Molecular (BNLMS), Institute of Chemistry, Chinese Academy of Sciences, Beijing 100080, PR China*
[b]*Graduate school of the Chinese Academy of Science, Beijing 100080, PR China*
[c]*Chemistry Department and Shanghai Key Laboratory of Molecular Catalysis and Innovative Materials, Fudan University, Shanghai 200433, PR China*
[d]*College of Chemistry, Jilin University, Changchun 130023, PR China*

Received 10 July 2006; received in revised form 19 September 2006; accepted 27 September 2006
Available online 29 September 2006

Abstract

Single-crystal nanowires of hexagonal tungsten trioxide in a large scale have been successfully prepared by a simple hydrothermal method without any templates and catalysts. Uniform h-WO_3 nanowires with diameter of 25–50 nm and length of up to several micrometers are obtained. It is found that the morphology and crystal form of the final products are strongly dependent on the amount of the sulfate and pH value of the reaction system. The electrochemical performances of the as-prepared h-WO_3 nanowires as anodic materials of Li-ion batteries have also been investigated. It deliveres a discharge capacity of 218 mAh g^{-1} for the first cycle. In addition, the cycle ability of the nanocrystals is superior to that of bulk materials, which implies the morphology and particle size have the influence on the electrochemical performances.

Keywords: Low-dimensional structures; Growth from solution; Nanomaterials; Semiconducting materials

1. Introduction

Among the numerous transition metal oxides, tungsten oxide is of intense interest due to its many known applications in electrochromic devices, gas sensors and photocatalysts [1–3]. Among various crystal structures of WO_3, hexagonal form of tungsten trioxide (h-WO_3) is of great interest owing to its well-known tunnel structure (Fig. 1) and has been widely investigated, especially as an intercalation host for obtaining hexagonal tungsten bronzes M_xWO_3 ($M = Li^+$, Na^+, K^+, etc.) and a promising material for negative electrodes of rechargeable lithium batteries [4]. Meanwhile, with the development of one-dimensional nanostructures, dimensionality and size of the materials have also been regarded as critical factors that may bring some novel and unexpected properties [5–12]. So the synthesis of WO_3 with well-controlled dimensionality, sizes and crystal structure is of special interest and of great importance.

Recently, many efforts have been focused on the exploration of new synthetic routes for the synthesis of tungsten oxide nanowires/nanorods, including electrochemically etching method [13], chemical vapor deposition [14–16], template directed synthesis [17,18], solution-based colloidal approach [19–21], and hydrothermal reaction [22,23]. However, most of the previous approaches only lead to the formation of monolinic $W_{18}O_{49}$ one-dimensional (1D) nanostructure. And the studies on 1D nanoscaled h-WO_3 are still rare due to the lack of preparation method for such materials. In addtiion, the investigation of the application of h-WO_3 with 1D

*Corresponding authors. Fax: +86 10 8261 6517.
E-mail address: jnyao@iccas.ac.cn (J. Yao).

0022-4596/$ - see front matter © 2006 Elsevier Inc. All rights reserved.
doi:10.1016/j.jssc.2006.09.020

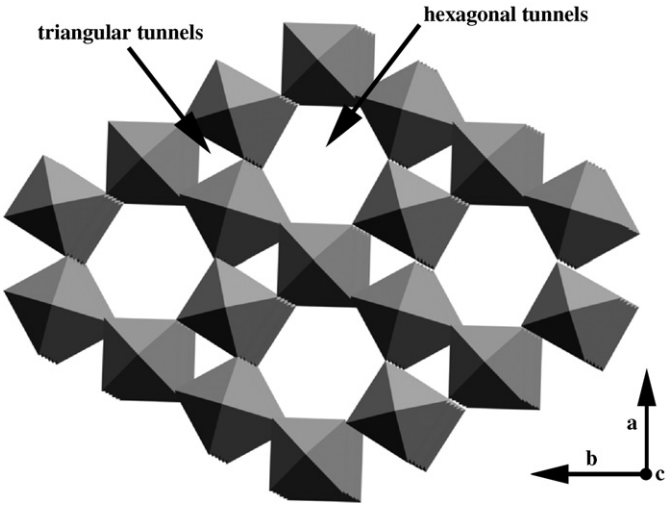

Fig. 1. Arrangement of [W-O_6] octahedral in the structure of hexagonal WO_3. Cross-section in the *ab*-plane perpendicular to the *c*-axis. Large and small open circles refer to positions in hexagonal and triangular tunnels, respectively.

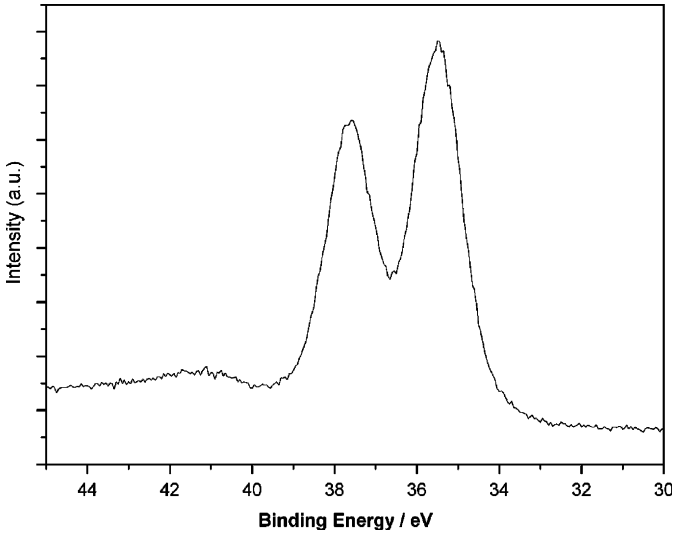

Fig. 3. W*4f* core-level XPS spectrum of the h-WO_3 nanowires.

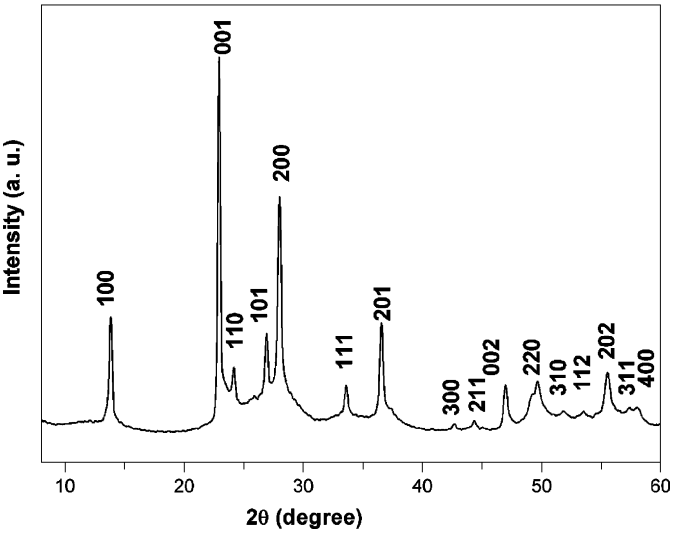

Fig. 2. XRD pattern of as-prepared products.

nanostructure as electrode materials is still rarely found in the literature until now. In this paper, we report a simple hydrothermal route to a large-scale synthesis of uniform single-crystalline nanowires of hexagonal tungsten trioxide without any templates or catalysts. The electrochemical performances of the as-prepared h-WO_3 nanowires as anodic materials of Li-ion batteries have also been investigated.

2. Experimental section

In a typical synthesis, lithium sulfate (1 g) was added to 20 ml of lithium tungstate solution (0.125 M, in distilled water). Then an aqueous solution of hydrochloric acid (3 M) was added dropwise to the mixture solution until the pH value of the solution reached 1.5. The mixture was then

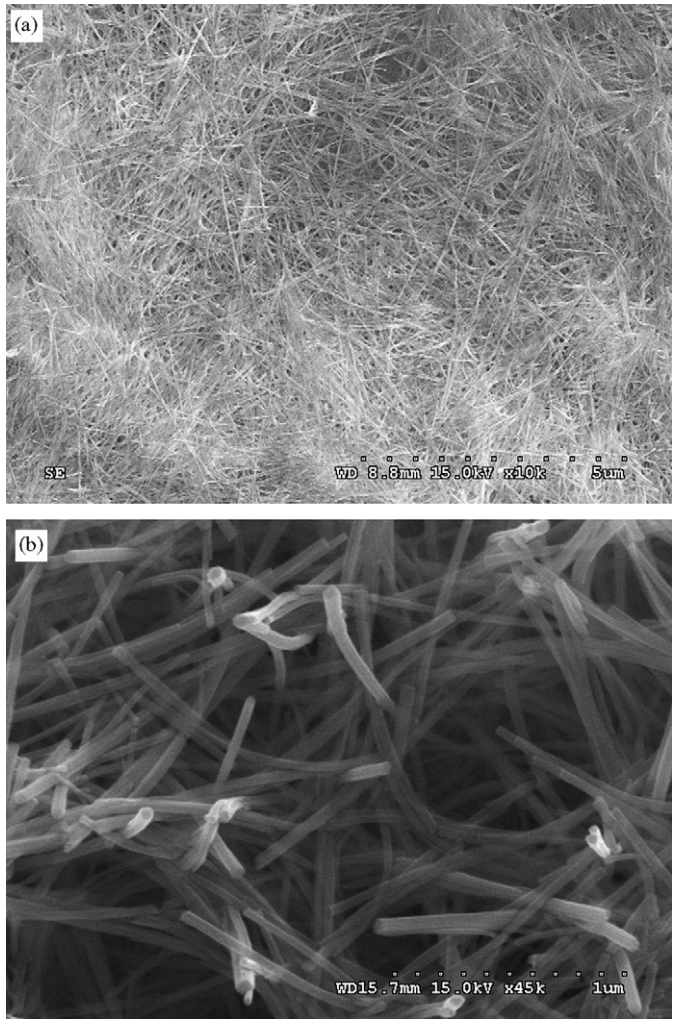

Fig. 4. Representative SEM images of as-synthesized tungsten oxide nanowires. (a) low magnification image; (b) high magnification image.

transferred into a Teflon-lined stainless steel autoclave and heated at 180 °C for 24–48 h. After reaction, the autoclave was then cooled to room temperature. The pressure maintained during the synthesis is about 9 atm. The pH value of the reaction system was found to increase to 1.8 after reaction. The final products were obtained by centrifugation and washed with deionized water and pure alcohol to remove ions possibly remnant in the final products, and dried at 60 °C.

X-ray diffraction (XRD) analysis was performed using a Japan Rigaku D/max-2500 diffractometer with Cu$K\alpha$ radiation ($\lambda = 1.5418$ Å) at a scan rate of $8^\circ\,\mathrm{min}^{-1}$. The sizes and shapes of the nanowires were observed on a field emission scanning electron microscope (SEM, Hitachi, S-4300) and high-resolution transmission electron microscope (HRTEM, JOEL JEM-2010 operated at 200 kV). XPS measurements were carried out with an ESCALab220i-XL spectrometer by using a twin-anode Al Kα (1486.6 eV) X-ray source. All the spectra were calibrated according to the binding energy of the adventitious C1 s peak at 284.6 eV. The base pressure was about $3*10^{-7}$ Pa. Nitrogen adsorption of the h-WO_3 nanowires were measured at 77 K with an ASAP 2010 micrometrics degassed at 250 °C for several hours under vacuum.

The electrode was fabricated by compressing a mixture of 85% active material (h-WO_3 nanowires), 10% conductive material (carbon black) and 5% binder (polytetra-

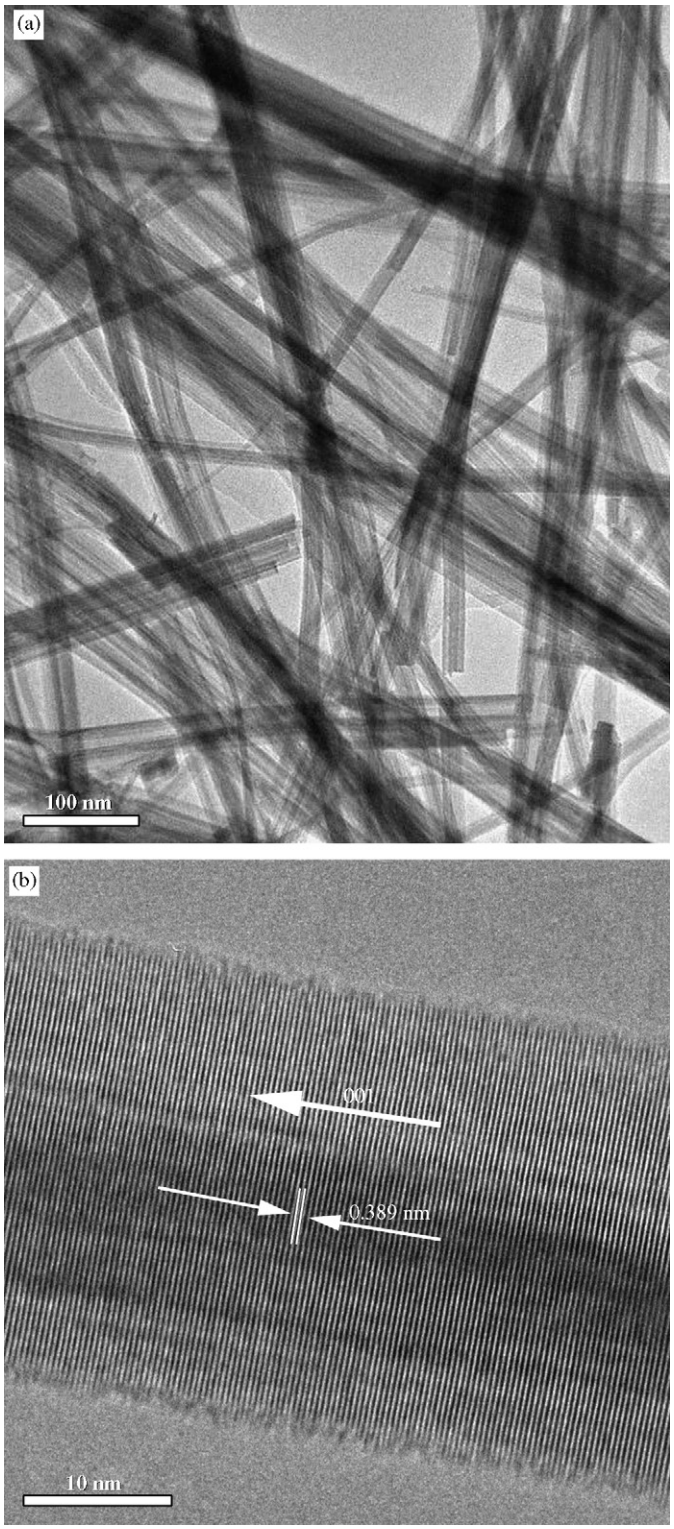

Fig. 5. (a) Overview TEM image of h-WO_3 nanowires; (b) HRTEM image of an individual nanowire with growth direction [001].

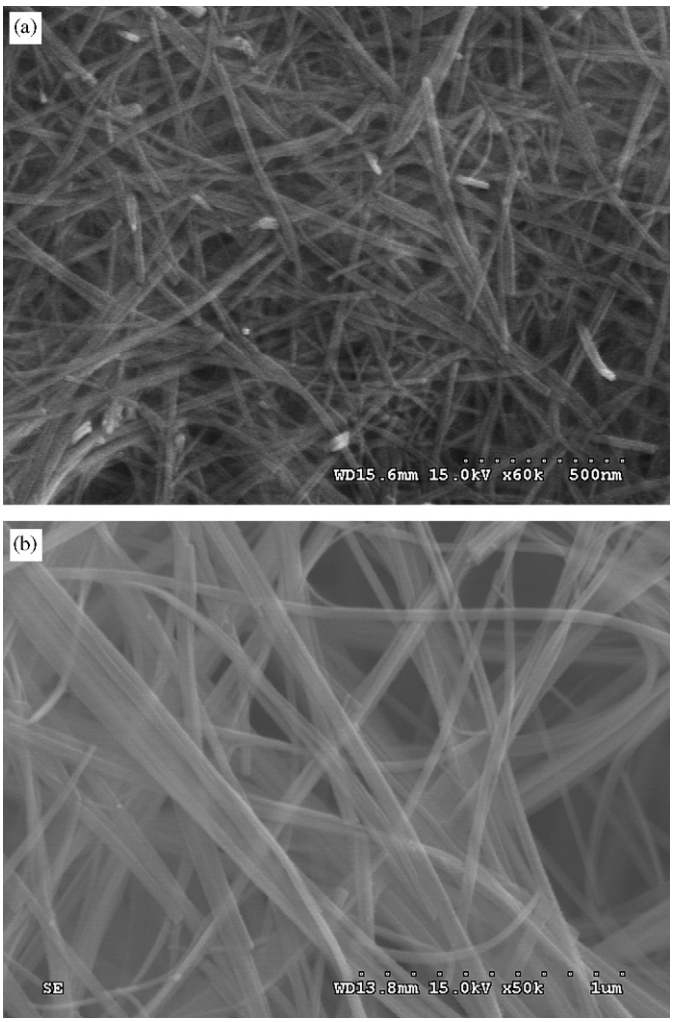

Fig. 6. SEM images for the intermediate products. (a) 6 h, (b) 48 h.

fluoroethylene, PTEE) on Nickel foam collector. Then the electrode was tailored to a disc of $\varphi = 12$ mm and dried at 80 °C for 12 h in a vacuum oven to remove the solvent and water. The cyclic voltammetry (CV) experiment was carried out at a scan rate of $0.5\,mV\,s^{-1}$ on Solartron 1287 Instrument using a three electrode system in which the lithium metal served as the counter and reference electrodes. The coin-type two electrode cells (CR-2032) fabricated by stacking of positive electrode, separator and negative electrode (lithium metal) were used in charge/discharge tests. All the tests were performed at room temperature using 1 M $LiPF_6$ dissolved in the mixture of ethylene carbonate (EC) and dimethyl carbonate (DMC) with the volume ratio of EC/DMC = 1:2 as the electrolyte.

3. Result and discussion

XRD pattern of the as-obtained products is shown in Fig. 2. All the diffraction peaks can be indexed to pure hexagonal phase of WO_3 with lattice constants of $a = 7.320$ Å and $c = 3.886$ Å, which agrees well with the reported values ($a = 7.289$ Å, $c = 3.889$ Å) from JCPDS card (33–1387). No peaks of impurities were detected from this pattern. The intensity of (001) peak increased distinctly in the obtained XRD pattern, implying the preferential growth of h-WO_3 along [001] axis. This supposition can be confirmed by HRTEM image. The chemical state of the tungsten and the oxygen/tungsten ratio in the samples are determined by X-ray photoelectron spectroscopy (XPS). Fig. 3 shows the typical XPS spectrum of the tungsten core level (W_{4f}) in the as-prepared products. The two peaks at 35.6and 37.7 eV in the spectrum can be attributed to $W_{4f\ 7/2}$ and $W_{4f\ 5/2}$, respectively, which are in good agreement with the reported values [27]. These two peaks are well separated without any shoulder, which indicates that all W atoms are in the +6 oxidization state. From the integrated areas of the tungsten (W*4f*) and oxygen (O*1s*) core level, we estimate the ratio of W/O in the products is about 1:3, which is in good agreement with XRD result. It is noting that the SO_4^{2-} ions were not found in the products from the XPS analysis.

The morphology of the as-synthesized products is observed using FE-SEM and low magnification TEM. The overall morphology of the sample is shown in Fig. 4(a), which shows that the sample is composed of a large quantity of uniform nanowires with diameters typically in the range of 25–50 nm and lengths of up to several micrometers. Close observations (Fig. 4(b) and Fig. 5(a)) reveal that these nanowires have a uniform diameter along their entire length and a narrow diameter distribution. To provide further insight into the structure of the as-prepared h-WO_3 nanostructures, an individual nanowire is analyzed by HRTEM measurement. As shown in Fig. 5(b), the regular spacings of the lattice fringes are found to be about 0.389 nm, corresponding to the (001) plane of h-WO_3 crystal. This confirms that the nanowires are single crystal which grow along the *c*-axis. The N_2 Brunauer–Emmett–Teller (BET) surface area of the as-prepared h-WO_3 nanowires is measured to be $33.8\,m^2\,g^{-1}$, confirming the small size and high surface area of the products.

Comparative experiments were carried out to investigate the influential factors on the growth of tungsten oxide nanowires. It is found that the reaction temperature and time had clear effects on the formation of nanowires. When the experiment was conducted at 120 °C, no products were obtained. However, h-WO_3 nanowires emerged when the

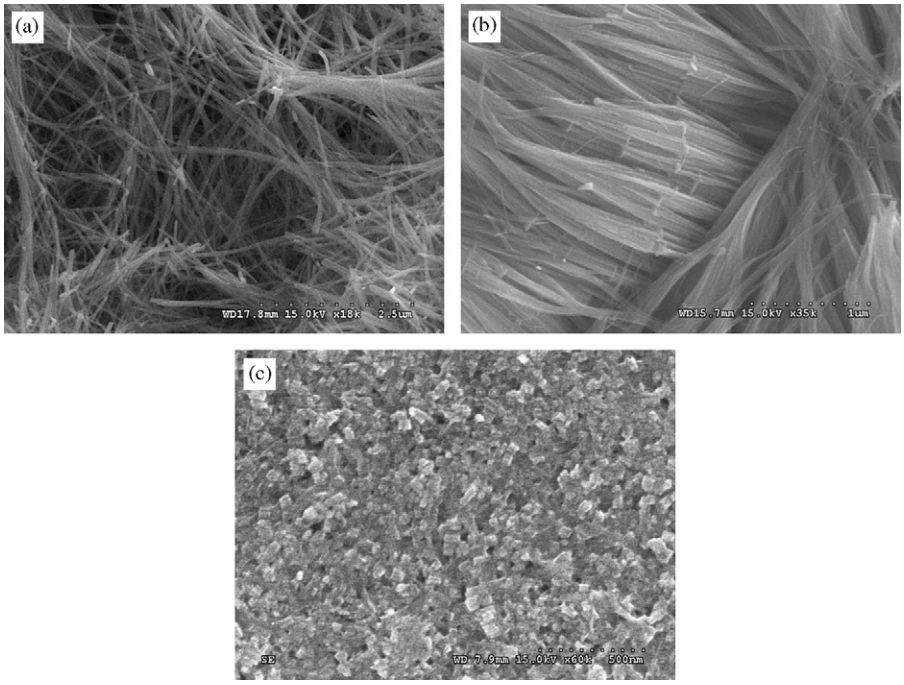

Fig. 7. SEM images for the products prepared at different pH value. (a) pH 1.6, (b)pH 1.2, (c) pH 0.5.

reaction was conducted at 150 °C. The optimum temperature for the rapid production of highly crystalline nanowire is as high as 180 °C. After reaction for 6 h, single-crystal nanowires of h-WO_3 in complete wire morphological yield had readily formed with diameter of 25–50 nm and length of up to several hundred nanometers. Further prolonging the reaction time up to 24 h, the length of the nanowires increased to a few micrometers. In addition, a few h-WO_3 nanowires had attached to one another through their side crystal planes during the reactions (Fig. 6).

The pH value and sulfates play important roles in determining the crystal structure and morphology of the final products. When the experiment was conducted at high pH value (>2), no products were obtained. The uniform h-WO_3 nanowires in a large-scale as well as pure hexagonal phase could be obtained when the reaction system was acidified to the pH range of 2.0–1.5. With a further decrease of pH value to the range of 1.4–1.0, the nanowires tend to aggregate each other resulting in the formation of bundle structures. (Fig. 7) When the pH value was lower than 0.5, the formation of nanoparticles is favorable. These results are a little different from that reported by Whittingham et al. In our experiment, the hexagonal phase of WO_3 can be obtained at pH 1–1.5 while only the mixture of unidentified phase was generated in their work at the same pH value. We believe that the reason of this difference is due to the addition of sulfate in our reaction system. These sulfates tend to induce the formation of hexagonal tungsten oxide, which may act as stabilizing ions for the hexagonal and triangular tunnels in the h-WO_3. Based on the experiment results, we believe that both the pH and the sulfate have the strong influence on the crystal structure of the products.

The sulfate also plays a crucial role in controlling the 1D growth of the final products. Controlled experiments have shown that without Li_2SO_4, only irregular particles were obtained. With an increase in the dosage of Li_2SO_4 to 0.5 g, the mixture of particles and nanorods was generated. The products in complete wire morphology can be obtained with 1 g of Li_2SO_4 added. The crystal form of the products also changed from orthorhombic phase to hexagonal phase with an increases of the amount of sulfate from 0.5 to 1.0 g. (Figs. 8 and 9) Excess amounts of the sulfate had no obvious effect on the wire morphology and crystal form. The details of the effect of sulfate on the formation of WO_3 nanocrystal is not clear up to date. However, it is well known that the anisotropic growth of the particles can be explained by the specific adsorption of ions to particular crystal surface, therefore, inhibiting the growth of these faces by lowering their surface energy. To investigate the influence of different ions on the formation of WO_3 naowires, other inorganic salts including $(NH_4)_2SO_4$, K_2SO_4, KNO_3 and LiBr were also tested in this work. Our results show that both $(NH_4)_2SO_4$ and K_2SO_4 induce the formation of the 1D nanostructures of h-WO_3. However, the addition of KNO_3 and LiBr only leads to the formation of microparticles. It is likely that only the sulfate could leads to the formation of WO_3 1D nanostructures, which may act as a capping agent to control the growing rate of different crystal faces through selective absorption. While other inorganic salts only induce the formation of irregular particles. Based on the

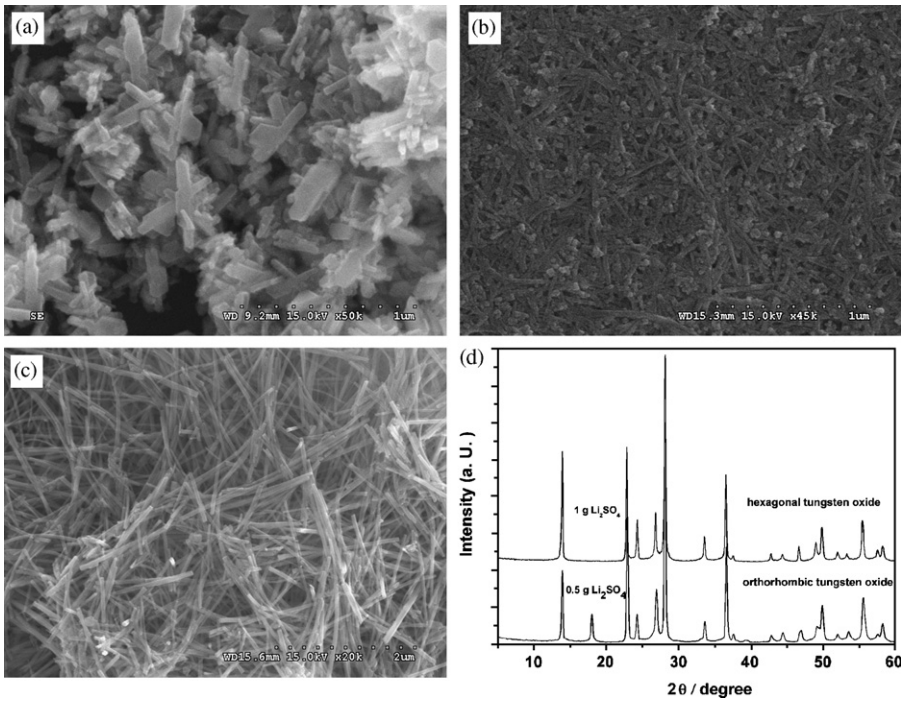

Fig. 8. SEM images and XRD pattern for the products prepared by adding different amount of Li_2SO_4. (a) 0 g, (b) 0.5 g, (c) 1 g, (d) XRD pattern for the products.

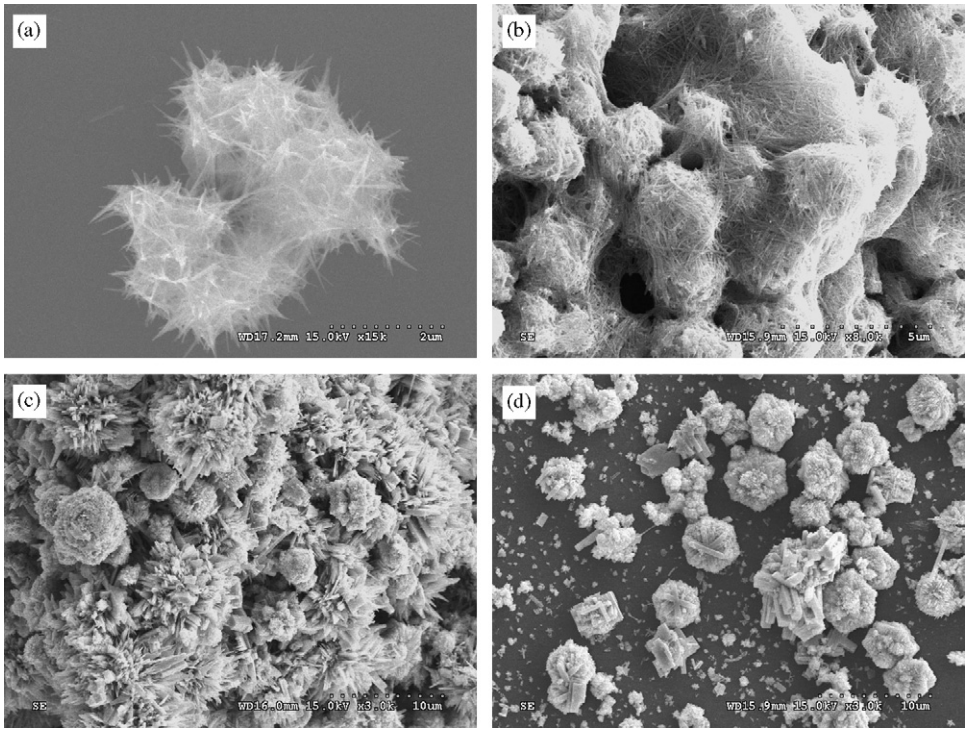

Fig. 9. SEM images for the products prepared by adding different inorganic salts. (a) $(NH_4)_2SO_4$, (b) K_2SO_4, (c) KNO_3, (d) LiBr.

above experiment results, the mechanism for the formation of WO_3 nanowires is speculated as follows:

The reaction to form WO_3 1D nanostructures can be formulated as:

$$Li_2WO_4 + 2HCl + nH_2O \rightarrow H_2WO_4 \bullet nH_2O + 2LiCl \quad (1)$$

$$H_2WO_4 \bullet nH_2O \xrightarrow[Li_2SO_4]{\text{Hydrothermal condition}} WO_3 + (n+1)H_2O \quad (2)$$

This novel method is based on treating the tungsten acid in the presence of Li_2SO_4 under hydrothermal conditions. In this reaction, with sufficient energy provided by the hydrothermal system, the WO_3 nuclei were quickly formed from the precursor. With the presence of Li_2SO_4, these nuclei serve as seeds and following grow along the [001] direction of h-WO_3 unit cell due to sulfate preferentially absorb on the faces parallel to the *c*-axis of the WO_3 nanocrystal, resulting in the formation of the nanowires. At the meantime, a certain amount of cation ions are required as stabilizing ions for the hexagonal and triangular tunnels in the formation of h-WO_3 [25,26].

Fig. 10 shows the cyclic voltammetry (CV) analysis of the as-prepared h-WO_3 nanowires at a scan rate of $0.5\,mV\,s^{-1}$ between 1.0 and 3.5 V. In the first cycle, the two cathodic peaks of lithium in the h-WO_3 nanowire electrode are observed at 2.5 and 1.5 V vs. Li^+/Li, which can be attributed to the irreversible reactions that from the impurities on the surface of the nanocrystals. Meanwhile, two broad anodic peaks are observed. In the second cycle, the two cathodic peaks disappeared resulting from the surface residual species is eliminated. Meanwhile, the anodic peaks shift a little to negative potential without obvious decay of peak intensity. The covered area of negative scan embranchment becomes more close to that of positive scan embranchment, which implies the promotion of current efficiency. After the second cycle the electrode demonstrates quite a reversible behavior. In the following cycles, there is no substantial change in the curve shape between 1.0 and 1.5 V. Our results are in good agreement with that of nanosized a-WO_3 particles reported by Garcia-Belmonte et al. [28].

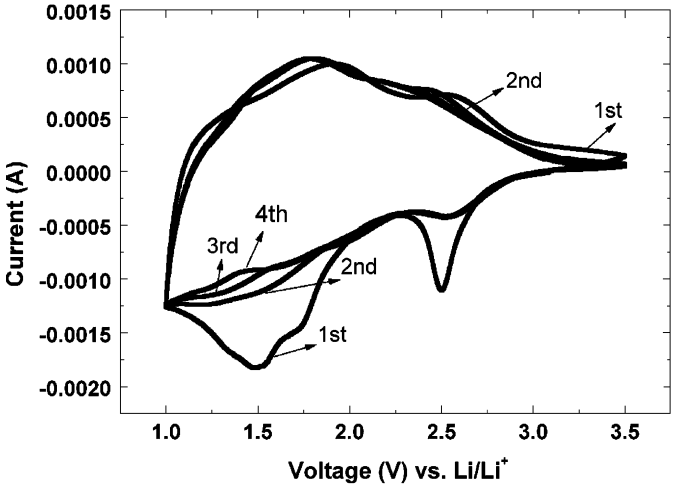

Fig. 10. Cyclic voltammetry (CV) of electrodes made by the as-prepared h-WO_3 nanowires at the 20 °C and a scan rate of $0.5\,mV\,s^{-1}$.

Fig. 11 presents the charge and discharge curves of the h-WO_3 nanowire electrode during the 1st and 2nd cycles at

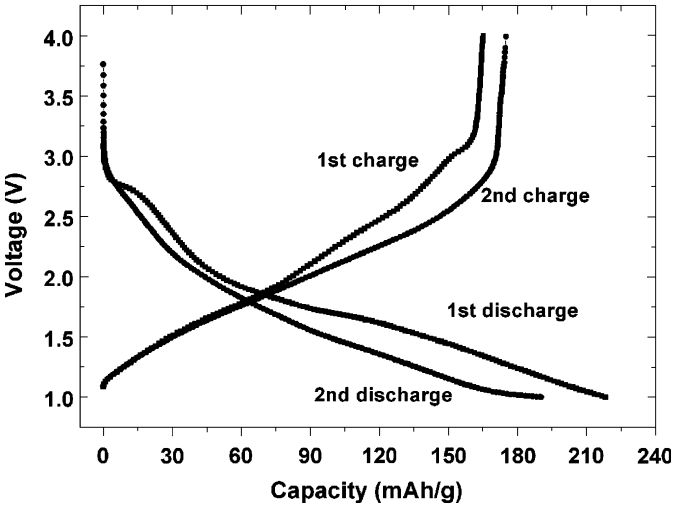

Fig. 11. Charge/discharge curves of the electrode made of as-prepared h-WO_3 nanowires at the current density of 50 mA g^{-1} and 20 °C.

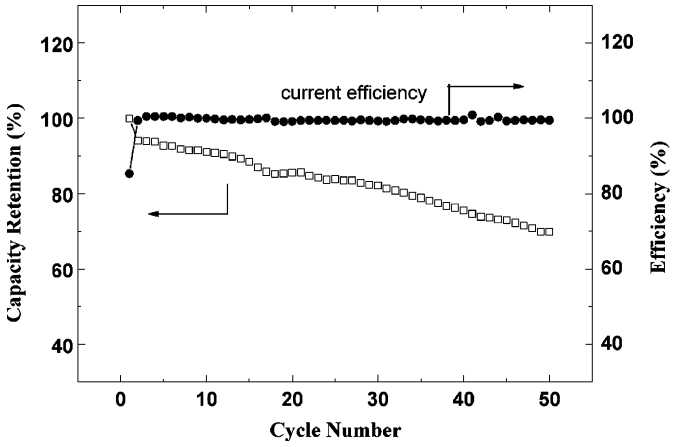

Fig. 12. Cycle life of the electrodes made by the as-prepared products at the current density of 50 mA g^{-1} and 20 °C.

the current density of 20 mA g^{-1} (0.1 C) between 1.0 and 4.0 V vs. Li/Li^+. In the discharge curve of the first cycle, there are two obvious potential slopes (2.6–2.75 V and 2.0–1.0 V vs. Li^+/Li). During the second discharge, only one discharge slope is observed in the range of 2.0–1.0 V, with a decrease of the discharge capacity. This change in potential range and irreversible capacity during the first and 2nd cycles are consistent with the above observation in the CV analysis. The discharge capacity of first cycle was 218 mAh g^{-1} and the charge capacity was 165 mAh g^{-1}, which shows the current efficiency of first cycle is 75.6%. However, this value increases to 92% at second charge/discharge cycle, which implies the large promotion of reaction reversibility of lithium intercalation/extraction in h-WO_3.

The cycle life was tested by charging/discharging the cell at a constant current of 50 mA g^{-1} between 1.5 and 3.0 V vs. Li/Li^+. The current efficiency remains over 99% during the cycle test. With an increase of the cycle numbers, the capacity decayed slowly, as shown in Fig. 12. After fifty cycles, the nanowires electrodes maintained about 75% of the initial capacity. However, it is noted that the h-WO_3 nanowires show a better cycle life than that of bulk materials, demonstrating that the morphology and the particle size have the influence on the electrode cycle life [24]. In general, the nanosized particles are able to expand much more easily and have better accommodation of the structural strain for the electrochemical reaction of lithium, resulting in improving cycle life [29]. Similar case have also been encountered in the a-Fe_2O_3 nanoparticles and SnO_2 nanofibers [30]. So we believe these nanosized h-WO_3 could be a promising material for Li-ion batteries.

4. Conclusions

In summary, we have exploited a low-temperature solution-based method to large-scale synthesis of h-WO_3 1D nanostructures. Highly pure wire-like h-WO_3 nanocrystals were synthesized successfully in gram quantities. These nanowires were evaluated as anodic materials for Li-ion batteries. These low-dimensional nanocrystals may also find potential applications in nanosensors, catalysis, microelectronic devices etc. We believe that this simple hydrothermal method, without any catalysts or templates, requiring no expensive equipment, and ensuring higher purity and uniformity of the products should be worth being explored further for other metal or semiconductor systems.

Acknowledgments

This work was supported by National Natural Science Foundation of China (No.50221201, 90301010, 50502033), and the Chinese Academy of Sciences.

References

[1] (a) M.S. Whittingham, Mater. Res. Soc. Bull. 14 (1989) 31;
(b) X.L. Li, T.J. Lou, X.M. Xiao, Y.D. Li, Inorg. Chem. 43 (2004) 5442.
[2] (a) T. He, Y. Ma, Y.A. Cao, X.L. Hu, H.M. Liu, G.J. Zhang, W.S. Yang, J.N. Yao, J. Phys. Chem. B 106 (2002) 12670;
(b) C. Santato, M. Odziemkowski, M. Ulmann, J. Auustynski, J. Am. Chem. Soc. 123 (2001) 10639.
[3] (a) M. Hibino, W. Han, T. Kudo, Solid State Ion. 135 (2000) 61;
(b) D.W. Murphy, P.A. Christian, Science 205 (1979) 651.
[4] (a) K.P. Reis, A. Ramanan, M.S. Whittingham, Chem. Mater. 2 (1990) 219;
(b) K.P. Reis, A. Ramanan, M.S. Whittingham, J. Solid State Chem. 96 (1992) 31;
(c) N. Kumagai, Y. Umetzu, K. Tanno, J.P.P. Ramos, Solid State Ionics 86–88 (1996) 1443–1449.
[5] Y.N. Xia, P.Y. Yang, Y.G. Sun, Y.Y. Wu, B. Mayer, B. Gates, Y.D. Yin, F. Kim, H. Yan, Adv. Mater. 15 (2003) 353.
[6] Y. zhou, S.H. Yu, X.P. Cui, C.Y. Wang, Z.Y. Chen, Chem. Mater. 11 (1999) 545.
[7] (a) J. Chen, L. Xu, W.Y. Li, X. Gou, Adv. Mater. 17 (2005) 582;
(b) F.S. Cai, G.Y. Zhang, J. Chen, X.L. Guo, H.K. Liu, S.X. Dou, Angew. Chem. Int. Ed. 43 (2004) 4212–4216.

[8] (a) X.F. Duan, C.M. Lieber, Adv. Mater. 12 (2000) 298;
(b) C.J. Barrelet, Y. Wu, D.C. Bell, C.M. Lieber, J. Am. Chem. Soc. 125 (2003) 11498.
[9] Z.W. Pan, Z.R. Dai, C. Ma, Z.L. Wang, J. Am. Chem. Soc. 124 (2002) 1817.
[10] (a) Z.R. Dai, Z.W. Pan, Z.L. Wang, J. Am. Chem. Soc. 124 (2002) 8673;
(b) J.Y. Lao, J.Y. Huang, D.Z. Wang, Z.F. Ren, Nano Lett 3 (2003) 235.
[11] (a) X.J. Cui, S.H. Yu, L.L. Li, L. Biao, H.B. Li, M.S. Mo, X.M. Liu, Chem. Eur. J. 10 (2004) 218;
(b) S.H. Yu, L. Biao, M.S. Mo, J.H. Huang, X.M. Liu, Y.T. Qian, Adv. Funct. Mater. 13 (2003) 639.
[12] G.T. Zhou, X.H. Wang, J.C. Yu, Cryst. Growth Des. 5 (2005) 1761.
[13] G. Gu, B. Zheng, W.Q. Han, S. Roth, J. Liu, Nano Lett 2 (2002) 849.
[14] B. Li, Y. Bando, D. Golberg, Adv. Mater. 15 (2003) 1294.
[15] C. Klinke, J.B. Hannon, L. Gignac, K. Reuter, P. Avouris, J. Phys. Chem. B 109 (2005) 17787.
[16] A.P.E. York, J. Sloan, M.L.H. Green, Chem. Commun. (1999) 269.
[17] B.B. Lakshmi, P.K. Dorhout, C.R. Martin, Chem. Mater 9 (1997) 857.
[18] B.C. Satishkumar, A. Govindaraj, M. Nath, C.N.R. Rao, J. Mater. Chem. 10 (2000) 2115.
[19] K. Lee, W.S. Seo, J.T. Park, J. Am. Chem. Soc. 125 (2003) 3408.
[20] M.J. Hudson, J.W. Peckett, P.J.F. Harris, J. Mater. Chem. 13 (2003) 445.
[21] (a) J. Polleux, A. Gurlo, N. Barsan, U. Weimar, M. Antonietti, M. Niederberger, Angew. Chem. Int. Ed. 45 (2005) 261;
(b) J. Polleux, N. Pinna, M. Antonietti, M. Niederberger, J. Am. Chem. Soc. 127 (2005) 15595.
[22] X.L. Li, J.F. Liu, Y.D. Li, Inorg. Chem. 42 (2003) 921.
[23] X.W. Lou, H.C. Zeng, Inorg. Chem. 42 (2003) 6169.
[24] S. Komaba, N. Kumagai, K. Kato, H. Yashiro, Solid State Ionics 135 (2000) 193.
[25] G.R. Patzke, A. Michailovski, F. Krumeich, R. Nesper, J.D. Grunwaldt, A. Baiker, Chem. Mater. 16 (2004) 1126.
[26] Z.J. Gu, Y. Ma, W.S. Yang, G.Z. Zhang, J.N. Yao, Chem. Commun. (2005) 3597.
[27] H. Qi, C.Y. Wang, J. Liu, Adv. Mater. 15 (2005) 411.
[28] J. Garcia-Canadas, I. Mora-sero, F. Fabregat-Santiago, J. Bisquert, G. Garcia-Belmonte, J. Electroanal. Chem. 565 (2004) 329.
[29] (a) A.S. Arico, P. Bruce, B. Scrosati, J.M. Tarascon, W.V. Schalkwijk, Nat. Mater. 4 (2005) 366;
(b) P. Poizot, S. Laruelle, S. Grugeon, L. Dupont, J.-M. Tarascon, Nature 407 (2000) 496.
[30] (a) D. larcher, C. Masquelier, D. Bonnin, Y. Chabre, V. Masson, J.B. Leriche, J.M. Tarascon, J. Electrochem. Soc. 150 (2003) A133;
(b) N. Li, C.R. Martin, B. Scrosati, Electrochem. Solid State Lett. 3 (2000) 316.